C. R. Physique 14 (2013) 553–563

Contents lists available at SciVerse ScienceDirect

Comptes Rendus Physique

www.sciencedirect.com

Trends and perspectives in solid-state wetting / Mouillage solide–solide : tendances et perspectives

Modeling dewetting of ultra-thin solid films

Modélisation du démouillage de films ultra-minces

Anna Chame [a,*], Olivier Pierre-Louis [b]

[a] *Instituto de Física, Universidade Federal Fluminense, 24210-340 Niterói, RJ, Brazil*
[b] *Institut Lumière Matière, UMR 5306, Université Lyon-1–CNRS, Université de Lyon, 69622 Villeurbanne, France*

ARTICLE INFO

Article history:
Available online 24 July 2013

Keywords:
Thin films
Diffusion
Wetting

Mots-clés :
Films minces
Difusion
Mouillage

ABSTRACT

We review some models for the dynamics of dewetting of ultra-thin solid films. We discuss the similarities and the differences between faceted and non-faceted systems. The faceting of the dewetting rim leads to corrections in the velocity of dewetting fronts both in flat and axisymmetric geometries. The faceting of the edge of the dewetting rim leads to a strong anisotropy of the dewetting instability. Faceting also induces novel dewetting regimes such as layer-by-layer dewetting, and monolayer dewetting.

RÉSUMÉ

Nous discutons quelques modèles pour la dynamique du démouillage de films solides ultra-minces. Nous discutons les similarités et les différences entre systèmes facettés et non facettés. Le facettage du bourrelet de démouillage mène à des corrections pour la vitesse de démouillage des fronts plans et des trous axisymmétriques. L'anisotropie influence aussi fortement l'instabilité morphologique des fronts de démouillage. Le facettage mène, par ailleurs, à de nouveaux regimes de démouillage, comme le régime couche par couche ou le démouillage des monocouches.

1. Introduction

In the past 15 years, much experimental effort has been devoted to the characterization of the dewetting (also called agglomeration) of thin solid films on solid substrates [1–5]. More recently, detailed experiments on monocrystalline films [6–14] have paved the way for a comparison with a theoretical description of these processes. SOI systems, i.e. single crystal Si/SiO_2, an important system for the semiconductor industry, have also been experimentally investigated by many authors [6,7,15,8,10–14]. In these studies a film of Si over SiO_2 retracts, forming a rim at the dewetting front (the rim being smooth or faceted). Then, the rim destabilizes (depending on its orientation), leaving an array of fingers where the front has passed. Finally, these fingers break down into droplets. Dewetting of metallic thin films has been investigated by many authors [5,9,12]. These systems dewet in a way that looks similar to Si/SiO_2 systems, with the initial formation of holes, which destabilize into arrays of dots. In summary, rim formation at the edge of a film or at the edge of a hole and rim instabilities are common features in solid-state dewetting, as well as the formation of facets [7,13]. However, some systems

* Corresponding author.
E-mail addresses: achame@if.uff.br (A. Chame), olivier.pierre-louis@univ-lyon1.fr (O. Pierre-Louis).

1631-0705/$ – see front matter
http://dx.doi.org/10.1016/j.crhy.2013.06.004

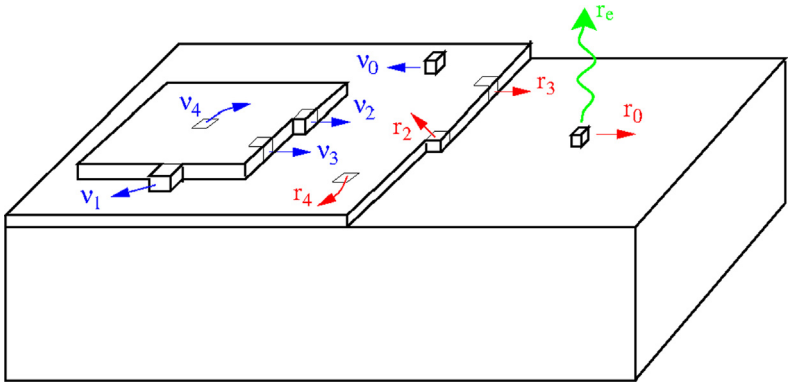

Fig. 1. (Color available online.) Schematics of the Kinetic Monte Carlo (KMC) model, with hopping rates ν_n and r_n, and sublimation rate r_e.

exhibit different morphologies, such as layer-by-layer dewetting of islands [16], or a labyrinthine pattern of islands (for very thin films of Ag on Si(111) [2]).

A large body of theoretical work have analyzed dewetting through continuum models based on the Mullins theory for surface diffusion [17], considering isotropic surfaces [18–20], including an effective wetting potential [21] and elastic effects [22,23], or by using an anisotropic surface energy [24]. Nevertheless, the presence of facets suggests that nucleation of new monolayer islands and motion of atomic steps play a crucial role in the dynamics.

Kinetic Monte Carlo simulations [25–27,29,30] have revealed that the dewetting process is indeed drastically influenced by the nucleation and dynamics of atomic steps on facets. As a consequence, we have developed a different approach based on a more microscopic description of the surface, including adatom diffusion and atomic step motion and nucleation, providing quantitative agreement with Kinetic Monte Carlo simulations [25–27,29,30].

In this short review, we list some of the main results of our approach, and we compare them with the results of the continuum model when they are available. We shall see in the following that our microscopic approach provides a number of results that only slightly differ from the continuum approach, and the distinction between the two approaches could therefore be difficult to measure in an experiment. This is for instance the case in the time dependence of the opening of a dewetting hole, or the retraction of a straight dewetting front. However, some characteristic behaviors of the two approaches are found. In addition, some phenomena cannot be handled by the continuum approach, such as layer-by-layer dewetting or the dewetting of a monolayer film, and must therefore be discussed within the frame of microscopic models.

2. Kinetic Monte Carlo simulations

In order to mimic experiments with a minimum number of ingredients, we have employed Kinetic Monte Carlo simulations [25,26]. We considered a solid-on-solid model on a square lattice (the substrate). For each site of this lattice, the film has an initial height $h = h_*$. The substrate, which is frozen, has $h = 0$. A particle of the film interacts with a first neighbor in the same plane through J, the lateral bond energy, and with its neighbor just below, through J_0, the vertical bond energy. If this neighbor belongs to the substrate, the bond energy is $J_0 - E_S$. In our model $E_S > 0$, so this bond is weaker. Another way to interpret E_S is by relating it to the spreading coefficient S [31] used in the context of wetting of liquids. It has been shown [29] that $E_S = E_{AV} + E_{AS} - E_{SV}$, where E_{AV}, E_{AS} and E_{SV} are respectively the interface adsorbate/vacuum, adsorbate/substrate and substrate/vacuum energies per site. This is just the same expression as the spreading coefficient with a minus sign. In this way, E_S can also be viewed as an excess interface substrate/adsorbate energy per site.

In the simulations, an epilayer atom with n neighbors in the same plane can hop to the nearest neighbor sites with rate:

$$\nu_n = \nu e^{-(nJ+J_0)/T} = \nu_0 e^{-nJ/T} \tag{1}$$

If this atom has a neighbor that belongs to the substrate, then the hopping rate is:

$$r_n = \nu e^{-(nJ+J_0-E_S)/T} = \nu_0 e^{-(nJ-E_S)/T} \tag{2}$$

where T is the temperature (in units of $k_B = 1$), and ν is an attempt frequency (see Fig. 1). We choose J as the energy unit, so that $J = 1$ in the following. Since J_0 appears in all rates, we write $\nu_0 = \nu e^{-J_0/T}$ and choose ν_0^{-1} as the time unit. Hence, in the following, we set $\nu_0 = 1$.

In our model, each particle at the film/vacuum interface has to break all its bonds to hop and can go to any of its four first neighbors, irrespective of height differences.

3. Heterogeneous dewetting from a straight front

The analysis of the dynamics of a dewetting straight front has been performed by Wong et al. [19]. There are two main results. First, the dewetting front is expected to retract, with a position given by $x \sim t^{2/5}$. This first result is easily understood

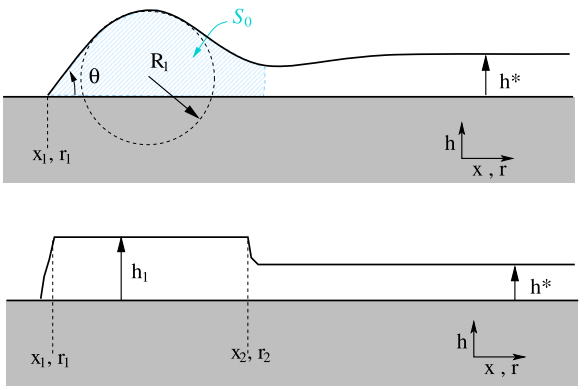

Fig. 2. Profile of a retracting film of initial height h_*. The triple line position is denoted by x_1 for a straight front, and r_1 for a circular hole. In the continuum model (see the top profile), the curvature radius of the rim is R_1 and its section is S_0 (hatched area). In our microscopic model (see the bottom profile), the rim facet is located between x_1 and x_2, and the rim has height h_1 and width ℓ.

from a qualitative analysis. We start with the Mullins model [17], which provides the evolution of the surface height as a function of the local geometry.

Exploiting the translational invariance of the system in the direction perpendicular to the front, we write down a one-dimensional equation for the height $h(x,t)$ of the surface as a function of the spatial variable x orthogonal to the front. Following Mullins [17]:

$$\partial_t h = \partial_x\left(D_S\left[1+(\partial_x h)^2\right]^{-1/2}\partial_x\left[\frac{\Omega\tilde{\gamma}}{T}\kappa\right]\right) \tag{3}$$

where D_S is the surface diffusivity, $\tilde{\gamma}$ is the surface stiffness, and Ω is the atomic volume. Both D_S and $\tilde{\gamma}$ depend on the local orientation. For simplicity, and following Wong et al. [19], we assume that the surface is isotropic, leading to:

$$\partial_t h = b\partial_x\left(\left[1+(\partial_x h)^2\right]^{-1/2}\partial_x\kappa\right) \tag{4}$$

where $\kappa = -\partial_{xx}h/(1+(\partial_x h)^2)^{3/2}$ is the surface curvature and $b = D_S\tilde{\gamma}\Omega/T$. In addition, we use the Young boundary condition at the triple line:

$$\partial_x h\big(x_1(t),t\big) = \tan\theta \tag{5}$$

where $x_1(t)$ is the triple line position and θ is the contact angle. Furthermore, we impose that no mass leaks from the island via the triple line to diffuse on the substrate, so that the total mass of the film is conserved.

Assuming that the rim has a height R_1 (see Fig. 2), Eq. (5) suggests a curvature $\sim 1/R_1$, and Eq. (4) then indicates that $\partial_t h \sim b/R_1^3$. In addition, since

$$\partial_t x_1(t) = \partial_t h(x_1)/\tan\theta \tag{6}$$

one has $\partial_t x_1(t) \sim b/(R_1^3\tan\theta)$. Moreover, mass conservation imposes that the increase of the rim section $\partial_t S_0$ equals the mass transferred from the film to the rim $h_*\partial_t x_1$, where h_* is the film thickness far from the dewetting front. Since the contact angle is imposed by Eq. (5), we expect $S_0 \sim R_1^2$. Combining these results, we find that:

$$x_1 \sim t^{2/5} \tag{7}$$

$$R_1 \sim t^{1/5} \tag{8}$$

An explicit solution exhibiting these scalings was obtained in Ref. [19] in the limit of small slopes.

Let us now discuss our Kinetic Monte Carlo simulation results in detail. The first striking observation is that the rim is faceted. Facets are extended surface singularities, where the r.h.s. of Eq. (3) is ill-defined. Indeed, the derivatives of the orientation $\partial_x h$ are ill-defined on a facet. In order to circumvent this difficulty, phenomenological models have been derived and used in the materials science community [32]. Here, we shall rather use a physicist approach: following the standard model of Burton, Cabrera and Frank [33], we resort to a more microscopic description, involving atomic step motion [34]. This modeling is based on the fact that atomic steps are thermodynamically well defined and non-singular lines on facets at equilibrium. In close-to-equilibrium conditions, the motion of atomic steps is driven by attachment and detachment of adatoms diffusing on atomically flat terraces between steps. The diffusion of adatoms is described by means of continuum diffusion equations. Such a semi-continuous framework, which proved to be a very efficient tool to describe the morphological evolution of crystal surfaces [33,34], breaks down only in far-from-equilibrium condition such as fractal

growth at low temperature, or fast etching, when surface diffusion does not have enough time to equilibrate the surface morphology at small scales [35].

In our model, we assumed again translational invariance along the direction of the triple line. We denoted by x_1 the position of the dewetting front, by h_1 the rim height at the frontier with the substrate, and at x_2 the rim ends: for $x > x_2$, the film has height h_*. We proposed a model to describe the temporal evolution of the front position x_1, of the rim width $\ell = x_2 - x_1$, and of the rim height h_1. A central assumption of the model is that mass transport is controlled by adatom diffusion on the top facet. This means that we assume that the other processes, such as the relaxation of the local profiles from $h = 0$ to $h = h_1$ around $x = x_1$, and from $h = h_1$ to $h = h_*$ around $x = x_2$, are faster than the evolution of the top facet width. We first need to find the concentration adatom profile c on the top of the rim ($x_1 \leqslant x \leqslant x_2$). Assuming diffusion limited mass transport on the rim facet, the concentration c obeys:

$$\nabla^2 c = 0 \tag{9}$$

where we assume that the concentration profile relaxes at times-scales much shorter than the rim evolution. Assuming local equilibrium, the concentrations at x_1 and x_2 are given by $c(x_1) = c_1 = c_{\mathrm{eq}} \mathrm{e}^{\Delta\mu/T}$ and $c(x_2) = c_2 = c_{\mathrm{eq}} = a^{-2}\mathrm{e}^{-2J/T}$. It can be shown [29] that the chemical potential at the edge of the film is $\Delta\mu = E_S/h_1$. Then the concentration profile is obtained as:

$$c(x) = c_1 + \frac{x - x_1}{\ell}(c_2 - c_1) \tag{10}$$

We expect that the temporal evolution of x_1 and x_2 is given by:

$$h_1 \partial_t x_1 = -a^2 D \partial_x c(x_1) + (x_2 - x_1)\partial_t h_1 \tag{11}$$

$$(h_1 - h_*)\partial_t x_2 = -a^2 D \partial_x c(x_2) \tag{12}$$

where D is the diffusion constant on the rim facet. The last term in Eq. (11) is a phenomenological term accounting for the possible increase of the rim facet height via nucleation of new layers.

Combining Eqs. (11), (12), and assuming that $x_1(t = 0) = 0$, the front position $x_1(t)$ can be written as a function of $h_1(t)$:

$$x_1 = \left(2a^2 D c_{\mathrm{eq}}\right)^{1/2} H_1^{-1} \left(\int_0^t \mathrm{d}t'\, H_1' \sigma' \right)^{1/2} \tag{13}$$

where $H_1 = (h_*^{-1} - h_1^{-1})^{-1}$, with h_* the initial film thickness, $\sigma = \exp[E_S/(T h_1)] - 1$, and $'$ indicates the substitution $t \to t'$.

With Eq. (13), we therefore have a description of the dynamics of the triple line as a function of the evolution of the rim height. If we assume that h_1 scales with time as a power law, we obtain:

$$x_1 \sim t^{(1-\alpha)/2} \tag{14}$$

$$h_1 \sim t^{\alpha} \tag{15}$$

Mass conservation then imposes that $\ell = x_1 h_*/(h_1 - h_*)$, leading to $\ell \sim t^{(1-3\alpha)/2}$. Note that the continuum model – Eqs. (4), (5) – imposes from the Young equation (5) that the width and the height of the rim scale in a similar fashion. If, following the continuum model, we impose $h_1 \sim \ell$, we would obtain $\alpha = 1/5$, in agreement with the continuum approach results – Eqs. (7), (8).

However, if we continue our microscopic approach based on step dynamics, the evolution of the rim facet height h_1 is not a power law. Indeed, h_1 increases via the nucleation of new layers on the rim. Considering that the first layer of the rim has already been created (by coalescence of the islands formed near the front), monolayer islands nucleate with rate $\mathcal{J}$ per unit length. These islands will grow and meet each other, and then a new layer will be completed. If $L_{\mathrm{nuc|zip}}$ is the typical distance between nucleation events and V_{zip} is the zipping velocity of the monolayer along the rim, then $L_{\mathrm{nuc|zip}} = (V_{\mathrm{zip}}/\mathcal{J})^{1/2}$. The height evolution then reads:

$$\partial_t h_1 = \mathcal{J} L_{\mathrm{nuc|zip}} \tag{16}$$

In order to obtain the height evolution, expressions for $\mathcal{J}$ and V_{zip} are therefore needed. To obtain $\mathcal{J}$, we used the two-dimensional nucleation theory. Following Ref. [26], the nucleation rate per unit length $\mathcal{J}$ is for $E_S \ll T h_1$, $T E_S \ll \pi \gamma^2 a^2 h_1$,

$$\mathcal{J} = \ell \frac{D c_{\mathrm{eq}}}{a^2} \left(\frac{E_S}{T h_1}\right)^{3/2} \left(\frac{T^2}{\pi \gamma^2 a^2}\right) \mathrm{e}^{-\pi\gamma^2 a^2 h_1/(T E_S)} \tag{17}$$

To evaluate V_{zip}, we considered that, for a monolayer island on the rim facet growing along the dewetting front, the only available length scale is the monolayer edge curvature κ. Then it is expected that:

$$V_{\text{zip}} \sim a^2 D c_{\text{eq}} \kappa \left(\frac{E_S}{T h_1} - \frac{a^2 \gamma \kappa}{T} \right) \tag{18}$$

The selected curvature is the one that maximizes the velocity: $\kappa = E_S/(2a^2\gamma h_1)$, so that:

$$V_{\text{zip}} \approx C_{\text{zip}} a^2 D c_{\text{eq}} \frac{E_S^2}{a^2 T h_1^2 \gamma} \tag{19}$$

where $C_{\text{zip}} \approx 0.25$ (determined from the simulations).

The precise expression of V_{zip} is actually not crucial. However, the fact that the nucleation rate $\mathcal{J}$ in Eq. (17) decreases exponentially with h_1 in our model has an important consequence: h_1 does not follow a power-law behavior, but rather behaves asymptotically as[1] $h_1 \sim \ln t$. If we substitute this behavior in Eq. (13), we find that:

$$x_1 \sim t^{1/2} (\ln t)^{-1/2} \tag{20}$$

$$h_1 \sim \ln t \tag{21}$$

In addition, from mass conservation $\ell = x_1 h_*/(h_1 - h_*)$, so that $\ell \sim t^{1/2} (\ln t)^{-3/2}$. Note that as opposed to the continuum model results where the rim is described by a unique length scale R_1, the microscopic model provides two length scales ℓ and h_1, which do not exhibit the same scaling behavior. The distinction between Eqs. (7), (8) and the results from the microscopic model is therefore related to the ability of distinguishing $(\ln t)$ from $t^{1/5}$. This is an important challenge for experiments.

The exact behavior of h_1 is actually more complicated than a simple exponential behavior. In order to check the validity of the microscopic model, the evolutions of h_1 and x_1 have been obtained by numerically solving Eqs. (13), (16) with $x_1 = x_2 = 0$ at $t = 0$. The solution is seen to agree quantitatively with KMC in Fig. 3a. (Note that this agreement relies on accurate evaluation of physical parameters in the KMC simulations, which is a non-trivial task in itself [25].)

To our knowledge, there are few systematic measurements of the rim position and height as a function of time. The first one was reported in Si/SiO_2 systems by Leroy et al. [13]. These authors observed the layer-by-layer increase of the height of the rim. Their measurement is consistent with $\alpha \approx 1/3$, leading to $x_1 \sim h_1 \sim t^{1/3}$, and ℓ constant. This surprising behavior questions both the continuum and the microscopic approaches. A second series of measurements were performed by Kim et al. [36], which are consistent with exponents of the continuum model with $\alpha = 1/5$. A precise comparison between these results and that of the microscopic model would be interesting.

The second main result of Wong et al. is the occurrence of film pinching due to the formation of a trench behind the rim. The observation from KMC simulations shows the absence of trench, and therefore the absence of pinching behind the rim. While it is tempting to speculate that the absence of trench behind the rim could be related to the presence of a nucleation barrier to form a two-dimensional monolayer hole in the film, we cannot provide a quantitative analysis at this point, and this is clearly an open question for future research.

4. Heterogeneous dewetting from pre-existing holes

In most experimental investigations, dewetting starts via heterogeneous nucleation on a localized defect, and a hole opens in the film. In order to address this regime, we consider an axisymmetric version of the models discussed above.

The situation with respect to the models is actually even more confusing in this case. Indeed, there exist not only two, but three hardly distinguishable results. First, one may simply extend the model of Wong et al. Indeed, for large enough holes, the curvature of the dewetting front should be irrelevant, and we should recover the scaling behavior of Eqs. (7), (8), leading to:

$$r_1 \sim t^{2/5} \tag{22}$$

$$R_1 \sim t^{1/5} \tag{23}$$

where r_1 is the rim hole radius, and R_1 is the height of the dewetting rim (which is once again assumed to scale in the same way as the rim curvature radius).

However, previous work by Srolovitz and Safran [18] find in the limit of small contact angles:

$$r_1 \sim t^{1/4} (\ln t)^3 \tag{24}$$

$$R_1 \sim t^{1/4} (\ln t)^{-1} \tag{25}$$

[1] Indeed, the evolution equation of h_1 takes the form $\partial_t h_1 = A(\ell, h_1) \exp[-\beta h_1]$, where A is an algebraic or logarithmic function of its arguments (i.e. no exponential dependence), and β is a constant. Such an equation can be integrated as $h_1(t) = \ln[\beta \int^t \mathrm{d}t' A(\ell, h_1)]/\beta$, up to an irrelevant arbitrary constant. Then, if h_1 and ℓ increase slower than $\exp[t]$ as expected, we may assume that $\int^t \mathrm{d}t' A(\ell, h_1) \sim t^\delta (\ln t)^\nu$ for large t, leading to $h_1(t) \sim \ln t$, up to corrections $\sim \ln \ln t$.

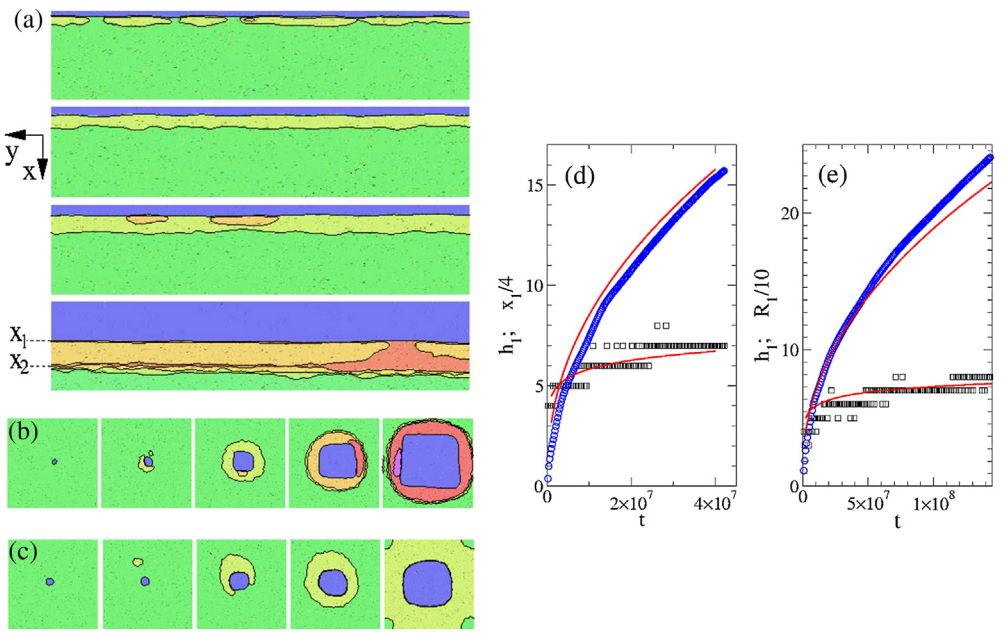

Fig. 3. (Color available online.) KMC simulations. (a) Dewetting from a straight front of position x_1, with a faceted rim. (b) Dewetting from a pre-existing hole of average radius r_1, with a faceted rim. (c) Dewetting from a pre-existing hole in the layer-by-layer regime. (d) Position x_1 and rim height h_1 for a straight front. Symbols: KMC with system size $L = 1000$, $T = 0.4$, $E_S = 0.5$, $h = 3$. Solid line: numerical solution of the model Eqs. (13), (16) without fitting parameter. (e) Rim height h_1 and radius r_1 of a hole with a faceted rim. Symbols: KMC with system size $L = 800$, $T = 0.4$, $E_S = 0.5$, and $h = 3$. Solid lines: numerical solution of an axisymmertic model similar to Eqs. (13), (16) without fitting parameter [26].

Srolovitz and Safran claim that the logarithmic corrections are related to the existence of a finite length scale h_* which hampers a simple power-law scaling, usually based on the existence of a unique growing length scale (here R_1) that dictates the full dynamics.

In addition, following the same lines as in the previous section, our microscopic model suggests [26]:

$$r_1 \sim t^{1/2}(\ln t)^{-1/2} \tag{26}$$

$$h_1 \sim \ln t \tag{27}$$

where h_1 is the height of the faceted rim. Using mass conservation, the rim width ℓ then obeys $\ell \approx r_1 h_*/(h_1 - h_*)$ for $\ell \ll r_1$, so that $\ell \sim t^{1/2}(\ln t)^{-3/2}$. Note once again that we have checked quantitatively the validity of the microscopic model, including pre-factors by comparison to our KMC simulations [26].

Our goal in this short review is not to decide which model is more appropriate, but to notice that different models provide different characteristic behaviors. One major open question in our opinion is to understand what are the conditions for the occurrence of each different scaling behavior.

An interesting result is that substitutions $\ln t \to t^{1/20}$ and $\ln t \to t^{1/5}$ allow one to recover the scaling – Eqs. (22), (23) – from the results of Srolovitz and Safran – Eqs. (24), (25) – or from our microscopic model for faceted rims – Eqs. (26), (27), respectively. Clearly, it is very difficult to distinguish $\ln t$ from $t^{1/20}$ in experiments or in simulations, and the difference between $\ln t$ and $t^{1/5}$ might also be delicate to analyze.

However, one possibility to check these models is to evaluate the relative dependence of the rim hole radius r_1 and the rim height R_1. For example, Eqs. (22), (23) constitute the only model that predicts that r_1/R_1^2 is a constant, Eqs. (24), (25) predict that $r_1 R_1^3$ is linear in time, and Eqs. (26), (27) predict that $r_1^2 h_1$ is linear in time.

Another regime seen in KMC simulations is the so-called layer-by-layer dewetting [26]. This regime is observed when E_S is small, h is large and when the distance between the holes is small, and is shown in Fig. 3c. Layer-by-layer dewetting is characterized by the nucleation of 2D islands on the film between the pre-existing holes, which spread on the surface to complete a new layer before the apparition of the next layer on the top of the islands. This regime is similar to the layer-by-layer increase of the height of ice islands observed in experiments [16]. A precise discussion of the conditions for this regime to occur is reported in Refs. [26,29]. Note that layer-by-layer dewetting of course has no counterpart in continuum models, which cannot account for the motion of a single atomic step.

5. Homogeneous nucleation and unstable films

Homogeneous nucleation of holes, i.e. formation of holes induced by thermal fluctuations, has been observed both in KMC simulations [26] and in experiments in Si(111)/a-SiO_2 [8] with film thicknesses $h_* < 4$ nm. In the early stages of

dewetting, this regime is characterized by a specific time dependence of the uncoverage θ, defined as the fraction of substrate surface uncovered by the dewetting process. Indeed, if the radius of a hole evolves as $r_1 \sim f(t)$, then the hole area behaves as $\sim f(t)^2$, and in the early stages where θ is small, the uncoverage results from the continuous formation of holes everywhere in the film, leading to $\theta \sim \int^t \mathrm{d}t' f(t')^2$. Hence, we expect from the models of Wong et al. – Eq. (22), Srolovitz et al. – Eq. (24), and Pierre-Louis et al. – Eq. (26) – mentioned above:

$$\theta \sim t^{9/5} \tag{28}$$

$$\theta \sim (t \ln t)^{3/2} \tag{29}$$

$$\theta \sim \frac{t^2}{\ln t} \tag{30}$$

Note that these predictions are based on the assumption that no instability develops. Once instabilities appear, the fronts destabilize to form arrays of fingers and move at constant velocity, i.e. $f(t) \sim t$, and $\theta \sim t^3$. In KMC simulations [26], the instability of the dewetting fronts indeed did not have enough time to develop during the dewetting process, and the homogeneous nucleation regime was characterized by an evolution of the uncoverage $\theta \sim t^{\vartheta}$, where $\vartheta \approx 2$, in approximate agreement with Eqs. (28)–(30). Simulation statistics were not large enough to distinguish between the three types of scaling from the measurement of θ. However, as discussed in the previous section, the opening dynamics of a single hole in KMC is in quantitative agreement with the microscopic model.

To our knowledge, detailed analysis of the nucleation barriers has not been performed. An interesting question would be to identify whether these barriers are different when the film surface is a facet, as in Ref. [26], or when the film surface is rough, in which case continuum models similar to the Mullins model (possibly supplemented with Langevin forces) should apply.

Another line of investigation is the study of dewetting of unstable surfaces. The instability can be triggered by anisotropy [21], by elastic stresses [22,23], or by attractive forces between the substrate and the surface [24].

6. Instabilities of solid dewetting fronts

In experimental studies with very thin SOI films (Si/SiO_2), the rim is unstable. This instability looks similar to the instability observed during the dewetting of liquid films [28]. As a result of the instability, large-scale-ordered arrays of solid islands emerging from the dewetting process were observed [6,15,8,10]. Usually, a rim forms at the edge of the film or at point defects, then destabilizes, leading to an array of fingers that finally break up into islands.

The stability of solid dewetting rims has been studied both from continuum models [20] and from microscopic models [27]. In both cases, the rim was found to be unstable. A schematics of the origin of the instability is shown in Fig. 4.

Let us start with the approach based on continuum models. In Ref. [20], the linear stability of a rim is discussed in the limit of small contact angles, leading to a most unstable wavelength:

$$\lambda_{\mathrm{m}} = \frac{2\pi h_*}{k_{\mathrm{m}}\theta} \tag{31}$$

where θ is the contact angle, and k_{m} depends implicitly on time via the front velocity. Fig. 6 of Ref. [20] suggests that $k_{\mathrm{m}}\theta \approx c(\partial_t x_1)^{1/3}$, where c is a constant around 0.1. Although this was not explicitly discussed in these terms in Ref. [20], we may use Eqs. (22), (23) in Eq. (31), leading to $\lambda_{\mathrm{m}} \sim t^{1/5}$.

Using the microscopic approach, one reaches a similar result. Indeed, once again, the instability arises from a rim which is growing. The stability analysis of the microscopic model leads to an asymptotic behavior of the wavelength of the mode of largest amplitude:

$$\lambda_{\max} \approx 2\pi \left(\frac{3 \int_0^t \mathrm{d}t' \, \tilde{\gamma}_1 h_{1(0)}^{-1}(t')}{\int_0^t \mathrm{d}t' \, E_{\mathrm{S}} h_{1(0)}^{-2}(t') \ell_{(0)}^{-1}(t')} \right)^{1/2} \tag{32}$$

where $\tilde{\gamma}_1$ is the effective stiffness per atomic layer of the rim facet edge near the triple line. (Note that in the continuum model description above, we should also use the wavelength of the mode with the largest amplitude $\lambda_{\max}$ which is the observable wavelength, instead of the wavelength of the most unstable mode λ_{m}. Due to the fact that perturbations grow on a rim which is not stationary, the amplitude of the perturbations obey an evolution equation with non-constant coefficients, and as a consequence the evolution of the amplitude of a given mode is not exponential. Therefore, strictly speaking, the mode of largest amplitude could be different from the fastest growing mode. However, we intuitively expect λ_{m} and $\lambda_{\max}$ to exhibit similar behaviors.) Using the scaling behavior identified in Eqs. (26), (27), one finds that in the microscopic model $\lambda_{\mathrm{m}} \sim t^{1/4}(\ln t)^{-1/4}$. From a numerical analysis of the microscopic model, the authors of Ref. [27] concluded that the behavior of the wavelength of largest amplitude indeed behaves effectively as $\lambda_{\max} \sim t^{0.2}$. Once again, note that the full solution of the microscopic model was found to be in quantitative agreement (including pre-factors) with the KMC simulations [27].

We may therefore conclude that, once again, the distinction between the two approaches could be delicate to measure in simulations and in experiments. However, both models conclude that there should be a coarsening of the wavelength of

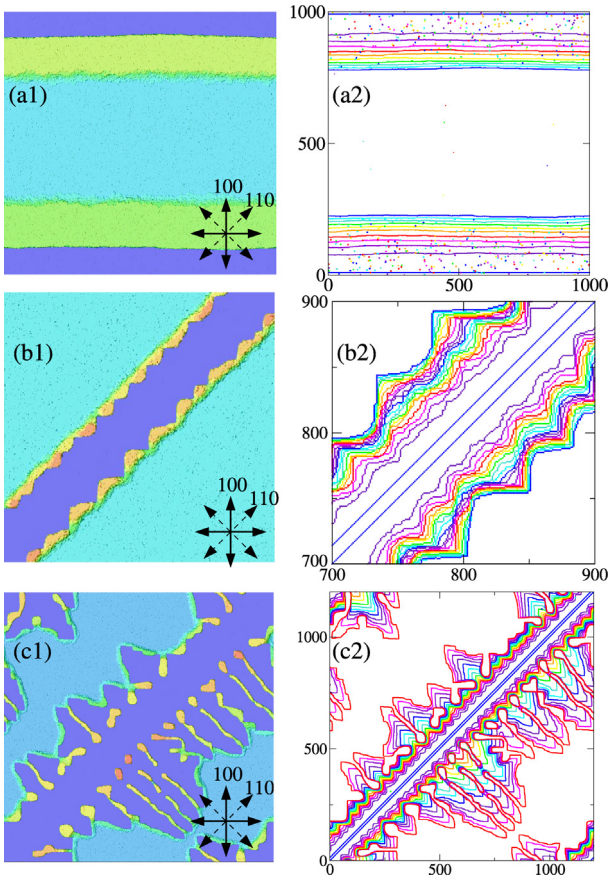

Fig. 4. (Color available online.) KMC simulations. Snapshots are presented in the left panels, here the gray-scale (blue–yellow–red color scale online) indicates the local height z. Right panels show the evolution of the film edge position x_1 as a function of time. Dewetting fronts are initiated by trenches along (100) in (a), along (110) in (b), (c). In all cases $T = 0.4$, and the initial height is $h = 3$. (a) A straight faceted rim forms, and no instability is observed for the (100) front, in a 1000×1000 system, with $E_S = 0.5$. (b) Zoom (200×200) at the early stages along (110). The typical wavelength of the instability increases with time: one observes coarsening. (c) Late time dynamics of (110) fronts. Fingers emerge from the rim instability. Parameters for: (b), (c) 1200×1200 system, with $E_S = 1.5$.

the instability in the initial stages. This observation is confirmed by KMC simulations, but there is up to now no detailed experimental observation of the early stages of the instability which would allow one to observe this coarsening behavior.

Both approaches claim that the wavelength that arises from this instability could control the distance between the fingers in the late stages of the instability. The heuristic analysis of Kan and Wong [20] provides reasonable orders of magnitudes as compared to experiments, and the microscopic approach of Dufay and Pierre-Louis [27] provides good agreement with KMC simulations. Using the two approaches, predictions have been proposed for the time of appearance of the instability, as discussed in Refs. [20,27].

Note that the microscopic approach allows one to discuss the anisotropy of the instability. Indeed, one may show that the effective stiffness per layer $\tilde{\gamma}_1$ increases exponentially with the rim height h_1 when the rim edge is faceted, leading to a restabilization of the front [27], in agreement with KMC simulations.

The anisotropy of the instability in KMC simulations is itself in very good agreement with the experiments on Si(100)/SiO_2 [10] when identifying the (100) orientation in KMC with the (110) orientation of Si. KMC simulations are indeed able to reproduce the observed shapes of unstable holes during dewetting, the anisotropy of the instability of straight fronts (stable fronts are oriented along the (100) direction with respect to the solid-on-solid lattice, while unstable ones are along the (110) direction [27]) and the formation and breakup of the fingers [10].

There is now need for comparison with other systems. Some recent results of Ye and Thompson [12] with Ni films on MgO indicate the formation of stable zigzag fronts. These results suggest that the linear instability that we have identified may not always lead ultimately to the formation of fingers.

7. Diffusion and evaporation

In high-temperature dewetting experiments of Si/SiO_2, islands resulting from the dewetting process were found to shrink [37]. This process could be driven by the reaction of Si with SiO_2, leading to the formation of SiO, which evaporates. In the

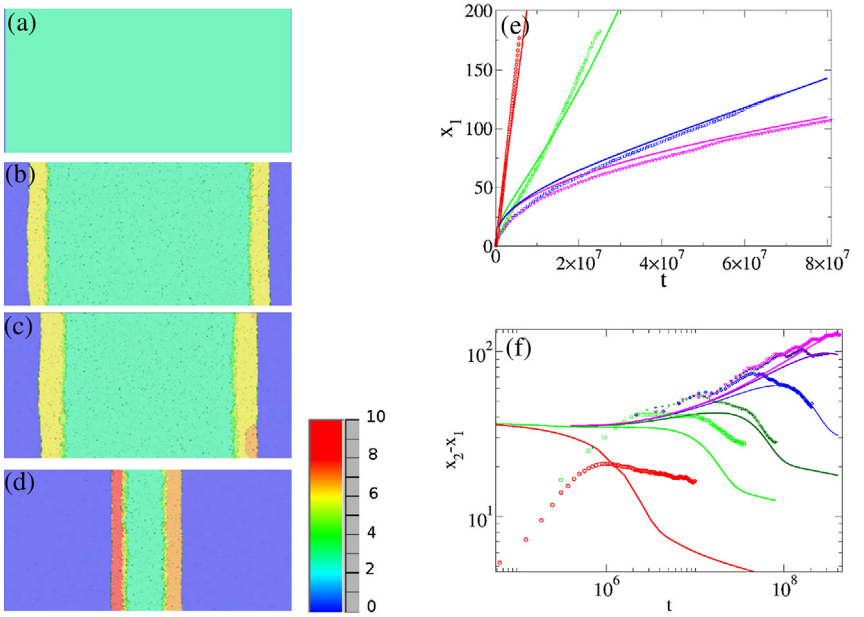

Fig. 5. (Color available online.) Left panels: sequence of snapshots of the dewetting dynamics with substrate evaporation observed in KMC. Right panels: temporal evolution of the rim position x_1 and of the rim width ℓ. In all cases $T = 0.4$, the initial height is $h = 3$ and $E_S = 0.5$. (a) We start from an initial trench in the film. (b), (d) Two dewetting rims form and move in opposite directions. Note that the rim width exhibits a maximum in the intermediate stages in (c). Simulation parameters: $E_{vs} = 5$, $L_x = 400$, $L_y = 800$. The z height scale of the surface is indicated on the right. (e) Front position x_1 for $E_{vs} = 3$ (red circles), 4 (green squares), 5 (blue squares), and 6 (magenta triangles). System size $L_x = 400$, $L_y = 400$. (f) Rim width for $E_{vs} = 3$ (red circles), 4 (green squares), 4.5 (dark green crosses), 5 (blue diamonds), 5.5 (purple crosses), and 6 (magenta triangles). System size $L_x = 800$, $L_y = 400$. Symbols are results from KMC simulations, and the solid lines represent the numerical solution of the model.

case of thin metallic films, the temperature can be raised close to the melting temperature [5,9], and the evaporation could also play a role.

Srolovitz and Safran [18] considered thin film dewetting in the presence of evaporation and condensation from a gas phase. They found that the dewetting front then moves at constant velocity.

We have studied a different regime from the microscopic approach, where atoms of the film may diffuse to the substrate, and then evaporate (or react) when they are on the substrate [30]. The only change in the model is that Eq. (11) should be replaced by:

$$h_1 \partial_t x_1 = -a^2 D \partial_x c(x_1) + (x_2 - x_1)\partial_t h_1 + v_s \tag{33}$$

where v_s is a mass flux accounting for the loss of mass from the film to the substrate. Interestingly, this model leads to a non-monotonous evolution of the rim width, which initially increases in a regime controlled by surface diffusion, and then starts to shrink when evaporation becomes relevant. This leads to a maximum of rim width at intermediate timescales. In the KMC simulations for this model, we considered also an evaporation rate:

$$r_e = \nu e^{-(J_0 + E_{vs} - E_S)/T} \tag{34}$$

where E_{vs} is the energy barrier for desorption of an atom in contact with the substrate. The analysis from the microscopic model is again in quantitative agreement with KMC simulations [30] in the substrate-mediated evaporation regime. (See Fig. 5.)

Since the regimes studied from the continuum model and the microscopic model were different, it is difficult to compare their conclusions here.

8. Dewetting of a monolayer film

Monolayer films are the smallest possible continuous layers. Their dewetting behavior is qualitatively different from that of thicker films [25]. Indeed, no rim forms during the dewetting of a monolayer. Instead, as shown in Fig. 6, we observed that a labyrinthine pattern of bilayer islands is formed during the dewetting process. We have studied in detail this behavior in Ref. [25]. Clearly, monolayer dewetting is beyond the scope of continuum models. Once again, we found that modeling based on atomic step motion is in agreement with KMC simulations, predicting the front velocity and the wavelength of the resulting structures. Since the dewetting front moves at constant velocity, we expect that during homogeneous nucleation $\theta \sim t^3$, as discussed in Section 5. This law is in agreement with KMC simulations [25].

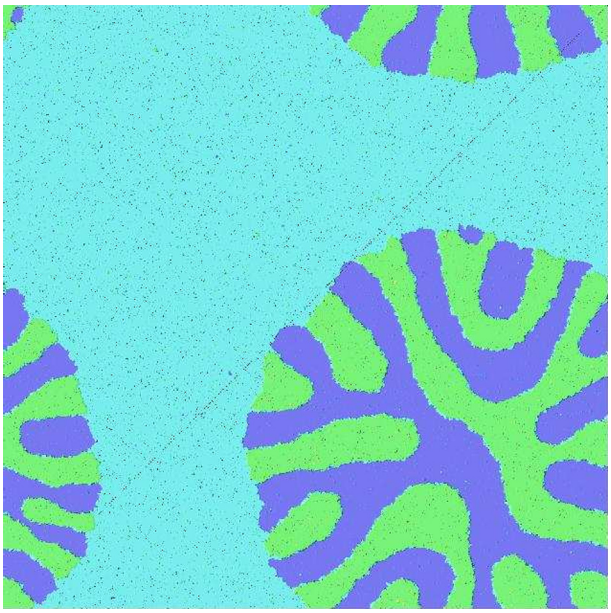

Fig. 6. (Color available online.) KMC simulation of monolayer dewetting. Color scale: dark-blue for $h = 0$, cyan for $h = 1$, green for $h = 2$. $T = 0.4$; $E_S = 0.1$; system size 1000×1000.

9. Conclusion

As a conclusion, we have discussed the modeling of dewetting processes in nanoscale thin films. There are basically two approaches. The first one is based on the implementation of the continuum model of Mullins. The second approach is based on a detailed study of the dynamics of atomic steps. The two approaches provide results that could be delicate to differentiate in experiments or simulations. The differences in the resulting scaling behaviors is related to the fact that two-dimensional nucleation is taken into account explicitly in the microscopic step models.

In the past five years, we have provided a detailed analysis showing that the microscopic approach provides a quantitative description of KMC simulations of dewetting. This modeling describes a regime of dewetting that is controlled by adatom diffusion, atomic step motion and two-dimensional nucleation. Although we have compared the results of our model to our own solid-on-solid KMC simulations only, we think that the main ingredients are generic, and should describe other KMC models and experiments when the rim is faceted. In some cases, the microscopic model is the only possible approach, such as in the so-called layer-by-layer dewetting [26], or in the dewetting of a monolayer [25].

In our opinion, there is still much work to be done in order to clarify the regimes where the continuum and microscopic models apply, but also to compare theories with experiments.

References

[1] E. Jiran, C.V. Thompson, Thin Solid Films 208 (23) (1992).
[2] K. Thürmer, E.D. Williams, J.E. Reutt-Robey, Phys. Rev. B 68 (2003) 155423.
[3] B. Krause, et al., J. Chem. Phys. 119 (2003) 3429.
[4] M. Coll, et al., Phys. Rev. B 73 (2006) 075420.
[5] E.J. Luber, B.C. Olsen, C. Ophus, D. Mitlin, Phys. Rev. B 82 (2010) 085407.
[6] B. Yang, et al., Phys. Rev. B 72 (2005) 235413.
[7] E. Dornel, et al., Phys. Rev. B 73 (2006) 115427.
[8] Z. Burhanudin, et al., Thin Solid Films 508 (2006) 235.
[9] H. Galinski, T. Ryll, P. Elser, J.L.M. Rupp, A. Bieberle-Hütter, L.J. Gauckler, Phys. Rev. B 82 (2010) 235415.
[10] E. Bussmann, F. Cheynis, F. Leroy, P. Müller, O. Pierre-Louis, New J. Phys. 13 (2011) 043017.
[11] F. Cheynis, E. Bussmann, F. Leroy, T. Passanante, P. Muller, Phys. Rev. B 84 (2011) 245439.
[12] Jongpil Ye, Carl V. Thompson, Acta Mater. 59 (2011) 582–589.
[13] F. Leroy, F. Cheynis, T. Passanante, P. Muller, Phys. Rev. B 85 (2012) 195414.
[14] M. Aouassa, L. Favre, A. Ronda, H. Maaref, I. Berbezier, New J. Phys. 14 (2012) 063038.
[15] D.T. Danielson, D.K. Sparacin, J. Michel, L.C. Kimerling, J. Appl. Phys. 100 (2006) 083507.
[16] K. Thürmer, N.C. Bartelt, Phys. Rev. Lett. 100 (2008) 186101.
[17] W. Mullins, J. Appl. Phys. 28 (1957) 333.
[18] D.J. Srolovitz, S.A. Safran, J. Appl. Phys. 60 (1986) 255.
[19] H. Wong, P.W. Voorhees, M.J. Miksis, S.H. Davis, Acta Mater. 48 (2000) 1719.
[20] W. Kan, H. Wong, J. Appl. Phys. 97 (2005) 043515.
[21] A.A. Golovin, M.S. Levine, T.V. Savina, S.H. Davis, Phys. Rev. B 70 (2004) 235342.
[22] A.A. Golovin, S.H. Davis, P.W. Voorhees, Phys. Rev. E 68 (2003) 056203.

[23] J.-N. Aqua, T. Frisch, A. Verga, Phys. Rev. B 76 (2007) 165319.
[24] M. Khenner, Phys. Rev. B 77 (2008) 245445;
M. Khenner, Phys. Rev. B 77 (2008) 165414.
[25] O. Pierre-Louis, A. Chame, Y. Saito, Phys. Rev. Lett. 99 (2007) 136101.
[26] O. Pierre-Louis, A. Chame, Y. Saito, Phys. Rev. Lett. 103 (2009) 195501.
[27] M. Dufay, O. Pierre-Louis, Phys. Rev. Lett. 106 (2011) 105506.
[28] R.V. Craster, O.K. Matar, Rev. Mod. Phys. 81 (2009) 1131.
[29] O. Pierre-Louis, A. Chame, M. Dufay, Eur. Phys. J. B 77 (2010) 57.
[30] A. Chame, O. Pierre-Louis, Phys. Rev. E 85 (2012) 011602.
[31] P.G. de Gennes, Rev. Mod. Phys. 57 (1995) 827.
[32] W.C. Carter, A.R. Roosen, J.W. Cahn, J.E. Taylor, Acta Metall. Mater. 43 (1995) 4309.
[33] W.K. Burton, N. Cabrera, F.C. Frank, Philos. Trans. R. Soc. Lond. Ser. A, Math. Phys. Sci. 243 (1951) 299.
[34] C. Misbah, O. Pierre-Louis, Y. Saito, Rev. Mod. Phys. 82 (2010) 981.
[35] A.L. Barabási, H.E. Stanley, Fractal Concepts in Surface Growth, Cambridge University Press, 1996.
[36] Gye Hyun Kim, Rachel V. Zucker, Jongpil Ye, W. Craig Carter, Carl V. Thompson, preprint, 2012.
[37] K. Sudoh, M. Naito, J. Appl. Phys. 108 (2010) 083520.